LAWRENCE
LIVERMORE
NATIONAL
LABORATORY

LLNL-TR-619598

Imaging scattered x-ray radiation for density measurements in hydrodynamics experiments on NIF

C. C. Kuranz

February 20, 2013

Disclaimer

This work performed under the auspices of the U.S. Department of Energy by Lawrence Livermore National Laboratory under Contract DE-AC52-07NA27344.

National Ignition Facility Concept Development Proposal: Imaging scattered x-ray radiation for density measurements in hydrodynamics experiments on the National Ignition Facility Final Report for Subcontract No. B598244

Carolyn C. Kuranz

The National Ignition Facility (NIF) is capable of providing enough energy to explore areas of physics that are not possible on any other laser system. This includes large-volume, geometrically complex hydrodynamic and radiation hydrodynamic experiments in which traditional, line-integrated radiographic techniques limit the quality of the results. As an example, we are involved in divergent hydrodynamic experiments at the NIF, motivated by supernova hydrodynamics, that cannot be diagnosed in detail with transmission radiography. We initially considered imaging x-ray scattering for this purpose and it appears feasible [1]. However, a better candidate is fluorescence imaging as the cross section of photoabsorption in the several-keV range is roughly 100 times larger than that of scattering. A single layer of the target will be uniformly doped with a fluorescent tracer, which will be pumped by a sheet of x-rays. The fluorescent intensity will be measured to create a density map of the doped material as it mixes with other layers. Developing this diagnostic will create a powerful tool to characterize hydrodynamic experiments with complex geometries.

1 Experimental setup

The fluorescence imaging setup will consist of three components: an x-ray backlighter ("the pump"), the target, and the detector. Emission produced by irradiating the backlighter will be filtered and collimated into a thin sheet. This sheet of x-rays will interact with the dopant atoms within a thin layer of the target by knocking out K-shell electrons. K-shell vacancies will be primarily filled by electrons from the L shell, producing K-α fluorescence which will be imaged by the detector. See Figure 1 for a simple schematic of the setup.

2 Target design

The target design used in this analysis is the same as published by Grosskopf et al [2]. Several different materials and configurations are discussed in a paper in preparation, but for this analysis we will only consider the Titanium-Foam-Foam (TFF) high-irradiance target. For this example we only look at solid densities, but the following method could be adapted to use the shocked densities.

The target will consist of three layers (see Figure 2). One hundred kJ of 351 nm wavelength laser radiation will be delivered to the inner layer of 0.598 mm thick, 4500 mg/cc Ti over 3 ns. The middle layer, composed of 1.395 mm thick, 500 mg/cc carbonized resorcinol formaldehyde (CRF) foam, will be doped with a fluorescent material. Doping the middle layer will allow both internal interfaces to be imaged via fluorescence. The outer layer will be 50 mg/cc CRF foam with a thickness of 5.499 mm. Each interface has a density drop of one order of magnitude.

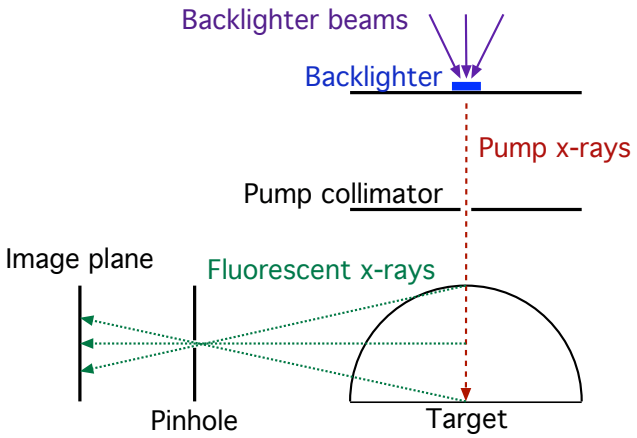

Figure 1: Schematic of setup (top view)

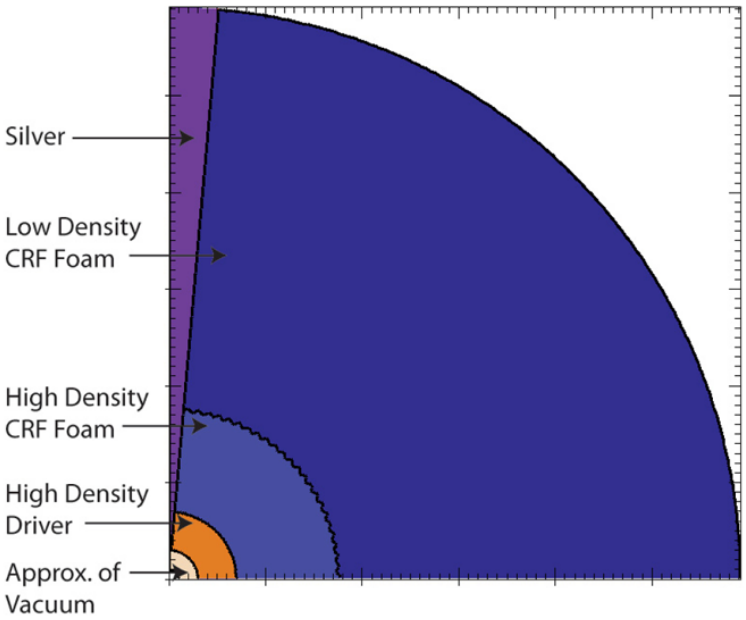

Figure 2: Initial target design for divergent hydrodynamic experiments. This model is for the high-irradiance case ($3 \times 10^{15}\ W/cm^2$) [2]

3 Measurements

Several measurements can be made utilizing this technique including mass density, flow velocity, electron density and ionization state. A brief discussion of each measurement follows.

3.1 Density map via fluorescent intensity

If the dopant atoms are uniformly dispersed throughout the middle layer of the target a density map can be created by imaging fluorescent intensity. This will allow the structure of the two interfaces to be imaged within the thin pumping layer. Multiple images could be taken of the target at different times to obtain more information about how the flow and instabilities develop. In order to use this technique successfully the differences in fluorescent intensity due to changes in density

must be large enough to detect. That is to say that the intensity shifts must be large compared to the noise on the detector.

3.2 Flow velocity via particle imaging velocimetry

If the dopant particles in the foam are large enough to be distinguishable in a 2D image they can be tracked by taking multiple snapshots of the plasma flow. This technique is known as particle imaging velocimetry (PIV), which is commonly used in fluid flow experiments [3]. Previous studies have had difficulties producing dopant granules small enough to move freely with the flowing material, a condition known as hydrodynamic invisibility [4]. Achieving hydrodynamic invisibility will require smaller dopant granules, in turn requiring an imaging system with higher spatial resolution to track individual particles.

3.3 Electron temperature and ionization state via blue-shifted K-α lines

Electron temperature along the shock can be measured using an imaging spectrometer. The spectral resolution of the spectrometer will need to be able to measure the blue shift in the K-α lines. More research will need to be conducted to see if this is feasible. The energy of the K-α radiation will be changed by the ionization state and will also need to be considered when looking at small changes in the spectrum. If these shifts are large compared to both the spectral resolution of the detector and the spread due to blue shift, the ionization state could be measured.

4 Fluorescent intensity

This section follows the work of N.E. Lanier et al to derive the fluorescent intensity for a given volume element within the target [4]. Here the appropriate changes have been made for the specified target geometry. The target geometry is shown in Figure 3, where $d_{1,in}$ and $d_{2,in}$ are the distances the x-ray must travel through each layer of CRF foam to reach the volume element with side length dx. Similarly, $d_{1,out}$ and $d_{2,out}$ are the distances traveled through each layer to escape the target. We only concern ourselves with volume elements within the high density CRF foam because it is the only doped layer.

Solving for these distances in terms of r and θ we find:

$$
\begin{aligned}
d_{1,in} &= \sqrt{R_i^2 - r^2\cos^2\theta} - r\sin\theta \\
d_{2,in} &= \sqrt{R_o^2 - r^2\cos^2\theta} - \sqrt{R_i^2 - r^2\cos^2\theta} \\
d_{1,out} &= \sqrt{R_i^2 - r^2} \\
d_{2,out} &= \sqrt{R_o^2 - r^2} - \sqrt{R_i^2 - r^2}
\end{aligned}
$$

where R_d is the outer radius of the driver, R_i is the radius of the interface between the two CRF foam layers, and R_o is the outer radius of the low density CRF foam.

The intensity of the pump x-rays that reaches a given volume element within the target, I_{elem}, is given by:

$$
I_{enter} = I_{pump,\lambda_p}\exp(-\mu_{1,\lambda_p}\rho_1 d_1)\exp(-\mu_{f,\lambda_p}\rho_f d_1)\exp(-\mu_{2,\lambda_p}\rho_2 d_2)\frac{\Omega_e}{4\pi} \tag{1}
$$

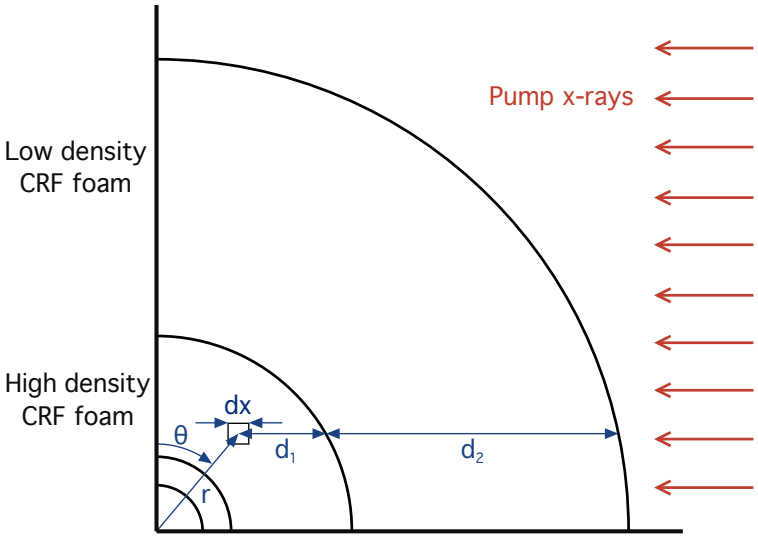

Figure 3: Diagram for intensity measurement derivation

where I_{pump,λ_p} is the intensity of the pump at wavelength λ_p, μ_1 is the attenuation coefficient of the low density CRF foam, μ_2 is the attenuation coefficient of the high density CRF foam mixed with the dopant, ρ is the density of the material, and Ω_e is the solid angle subtended by the volume element.

Intensity of fluorescence radiated by the volume element is given by:

$$I_{elem} = I_{enter} f_{K\alpha}[1 - \exp(-\mu_{f,\lambda_p}\rho_f dx)] \tag{2}$$

$$\approx I_{enter} f_{K\alpha}\mu_{f,\lambda_p}\rho_f dx \tag{3}$$

where $f_{K-\alpha}$ is the fraction of absorbed x-rays that are emitted as K-shell fluorescence, μ_{f,λ_p} is the photoelectric absorption coefficient of the fluorescent material at the pump wavelength, ρ_f is the density of the dopant, and dx is the characteristic length of the volume element. Note that μ for the fluorescent material is the photoelectric absorption, while it is the total attenuation for the bulk material. This is because we are only concerned about radiation absorbed by the dopant atoms because scattered radiation will not contribute to fluorescent signal. The approximation that dx is very small allows us to take only the first two terms in the expansion of I_{elem}.

The intensity reaching the detector, I_{det,λ_f}, is given by:

$$I_{det,\lambda_f} = I_{elem} \exp(-\mu_{1,\lambda_f}\rho_1 d_1) \exp(-\mu_{f,\lambda_f}\rho_f d_1) \exp(-\mu_{2,\lambda_f}\rho_2 d_2) \frac{\Omega_a}{4\pi} \tag{4}$$

where Ω_a is the solid angle subtended by the detector aperture.

Combining the previous equations we arrive at the final expression for the intensity of fluorescent radiation at the detector:

$$I_{det,\lambda_f} = I_{pump,\lambda_p} \exp[-(\mu_{1,\lambda_p} + \mu_{1,\lambda_f})\rho_1 d_1] \exp[-(\mu_{1,\lambda_p} + \mu_{1,\lambda_f})\rho_f d_1] \exp[(\mu_{2,\lambda_p} + \mu_{2,\lambda_f})\rho_2 d_2] f_{K\alpha}\mu_{f,\lambda_p}\rho_f dx \frac{\Omega_a \Omega_e}{(4\pi)^2} \tag{5}$$

To calculate the number of photons reaching each spatial resolution element of the detector we need to estimate the photon flux created by the backlighter. A rough estimate of the number of x-rays produced is:

$$N_{pump} = \frac{E_L}{h\nu}\eta_x = \frac{E_L\lambda}{hc}\eta_x \tag{6}$$

where E_L is the energy of the pump laser, h is Planck's constant, c is the speed of light, ν and λ are the frequency and wavelength of the pump x-rays, and η_x is the conversion efficiency of the backlighter. With the assumption that the pump x-rays come in as a sheet, we multiply the x-rays into bins corresponding to the spatial resolution of the detector:

$$N_{det} = N_{pump}\frac{dx}{2R_o}\exp[-(\mu_{1,\lambda_p} + \mu_{1,\lambda_f})\rho_1 d_1]\exp[-(\mu_{2,\lambda_p} + \mu_{2,\lambda_f})\rho_2 d_2] f_{K\alpha}\mu_{f,\lambda_p}\rho_f dx\frac{\Omega_e\Omega_a}{(4\pi)^2} \tag{7}$$

where R_o is the outer radius of the target.

5 Simulation results

CRF foam is roughly 93% carbon and 7% hydrogen, oxygen, and nitrogen by mass [5]. Here we assume that the absorption and scattering of x-rays is not significantly affected by nanostructures within the foam. This assumption is based on the idea that the wavelength of the x-rays is on the order of the atomic diameter of carbon (10 keV x-ray: 0.12 nm, carbon diameter 0.14 nm), so we expect that the interactions occur on an atomic scale rather than a molecular scale.

To estimate the fluorescent intensity it is assumed that the CRF foam is purely carbon. Over the range of relevant photon energies (5 - 15 keV) the x-ray attenuation is dominated by photoelectric absorption (see Figure 4) [6]. Incoherent scattering becomes significant near 15 keV and may need to be considered if high energy x-rays are required.

5.1 Attenuation of pump and fluorescent x-rays

Using equation (5) we can calculate the x-ray attenuation for each point in the pumped plane. Here we have taken $I_{pump,\lambda_p} f_{K\alpha}\frac{\Omega_e\Omega_a}{(4\pi)^2}$ to be unity for simplicity. Note that these simulations did not use the approximation made by equation (3) due to the minor difference in complexity.

These simulations show that higher energy x-rays are attenuated less by target material. Note that moving to higher energy pump x-rays results in a lower number of pump x-rays due to the higher energy cost per photon.

5.2 Effect of varying dopant density

The dopant density must be high enough to achieve an acceptable fluorescent intensity at the detector, but if the density must not be so high that the doped material absorbs a significant fraction of the pump radiation. If the second situation occurs there will be a significant drop in signal as the pump intensity is reduced in regions further from the source. This effect is shown in Figure 6.

In these simulations the bottom row shows the fluorescent intensity that reaches the detector from each point in the pump plane. The ideal case would have a uniform intensity throughout the middle layer, meaning the same pump intensity reaches each scattering volume. It is clear that 50 mg/cm^3 is too high for this reason, but there is only a small difference between the 0.5 and 5.0

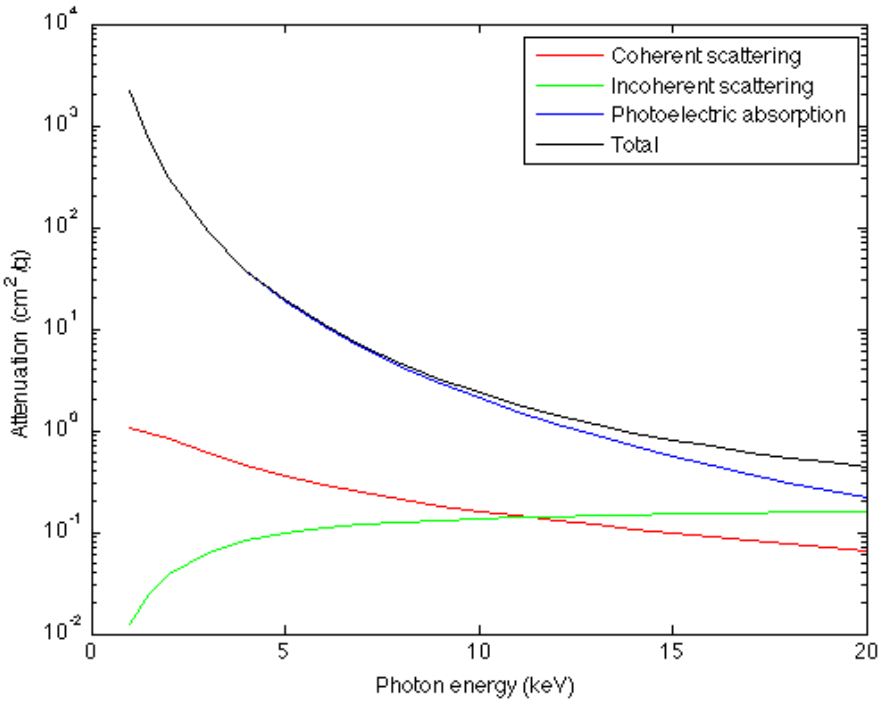

Figure 4: Attenuation coefficient for pure carbon [6]

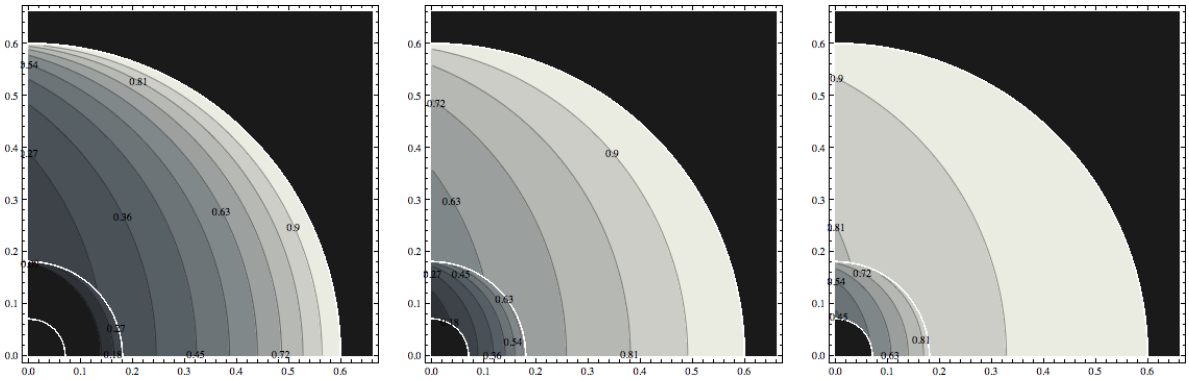

(a) Ti pumped Sc (b) Fe pumped Mn (c) Zn pumped Cu

Figure 5: Transmission of pump and fluorescent x-rays through each point of the target

mg/cm^3 for these elements. Note that the bottom row only shows relative intensities (normalized to the highest intensity for each case), a quantitative analysis will be needed to determine the required parameters when the detector requirements are known.

6 Proof-of-principle experiments

6.1 1D Target

Target design by Eliseo Gamboa in internal report shown in Figure 7 [7].

A simple 1D target will be used to provide a proof-of-principle for the fluorescent imaging

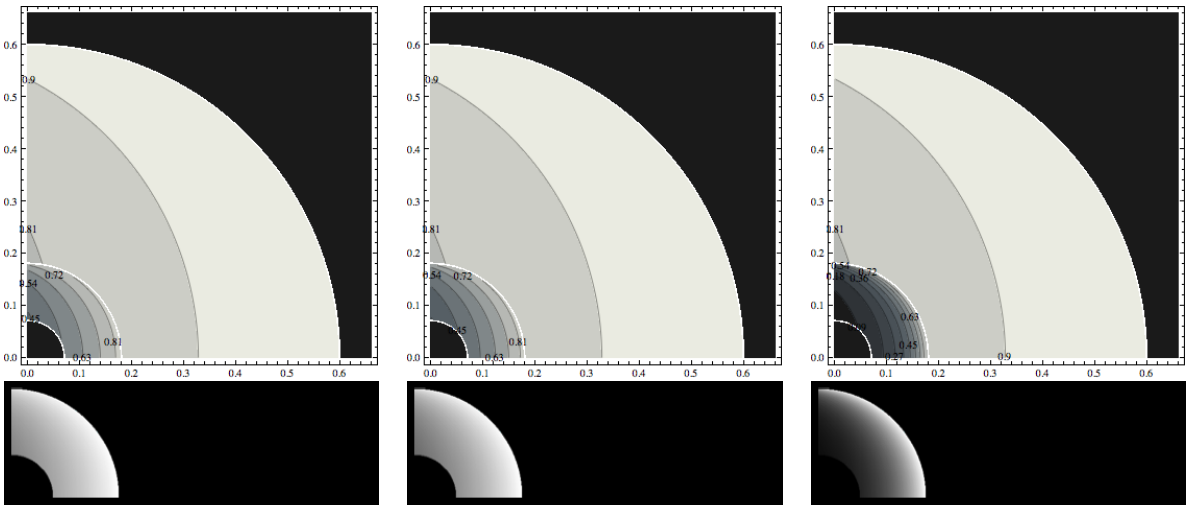

(a) 0.5 mg/cm^3 (b) 5 mg/cm^3 (c) 50 mg/cm^3

Figure 6: (top) Transmission of pump and fluorescent x-rays through each point of the target. (bottom) Fluorescent intensity reaching the detector normalized to the pixel with the highest intensity. All figures show Zn pumped Cu.

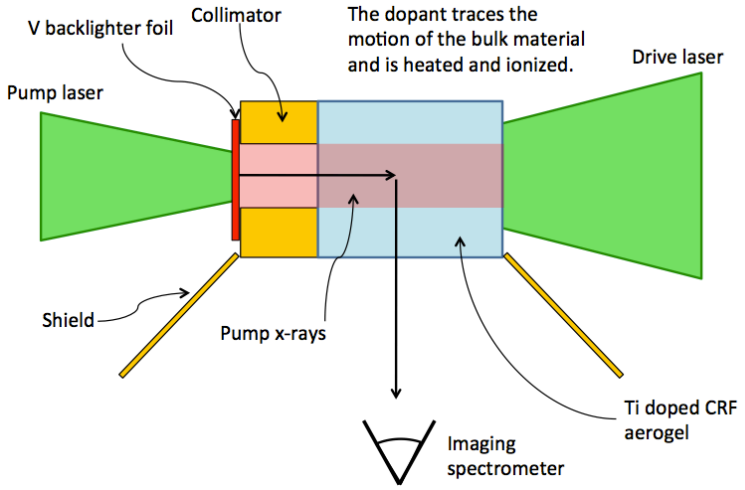

Figure 7: 1D target design [7].

techniques described above. 1D shocks have been well studied by the group, providing a good starting point that will minimize problems unrelated to the fluorescent diagnostic.

Filtering requirements, detector settings, and other important aspects of the experiment can be worked out with such a target, which will save time and money before moving to the spherically divergent case.

6.2 Planar divergent target

A divergent explosion experiment may be possible on facilities with less energy than NIF if the flow is constrained to a single diverging angle. This concept needs to be examined more closely to determine the laser characteristics required to drive instabilities using this design. See Figure 8 for

target geometry.

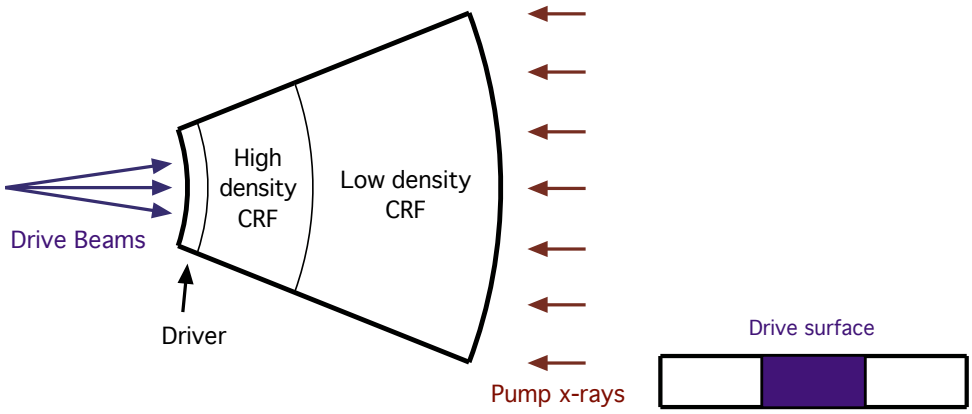

(a) Top view (b) Drive view

Figure 8: Planar divergent target design

This target may provide a platform to study divergent systems before time on NIF is scheduled. The angle of divergence and height of the target can be tuned based on experimental goals and energy available.

7 Conclusions and Future Directions

We have completed a analysis of an x-ray fluorescence diagnostic for a solid density, multi-layer target in a divergent geometry. We have also designed a proof-of-principle experiment to test this technique at a smaller facility. It may also be possible to do a scaled target to test the diagnostic technique at the Omega Laser Facility. The findings in this report are currently in preparation for publication by University of Michigan graduate student Michael MacDonald. Michael has presented these results at the American Physical Society Division of Plasma Physics Meeting, the Michigan Institute for Plasma Science and Engineering Symposium and the Defense Threat Reduction Agency Basic Research Technical Review. Finally, we plan to apply for experimental time at smaller facilities (laser facilities and light sources) in order to test this technique. A more specific experimental configuration will have to be detailed for each type of facility.

8 Acknowledgements

This work was funded primarily by the Lawrence Livermore National Laboratory under Subcontract B598244. Additional support was provided by the NNSA- DS and SC-OFES Joint Program in High-Energy-Density Laboratory Plasmas, grant number DE-FG52-09NA29548, the National Laser User Facility Program, grant number DE-NA0000850, and the Predictive Sciences Academic Alliances Program in NNSA-ASC via grant DEFC52- 08NA28616.

References

[1] C.M. Huntington, C.M. Krauland, C.C. Kuranz, S.H. Glenzer, and R.P. Drake. Imaging scattered x-ray radiation for measurement of local electron density in high-energy-density experiments. *High Energy Density Physics*, 6(2):194–199, 2010.

[2] M.J. Grosskopf, R.R. Drake, C.C. Kuranz, A.R. Miles, J.F. Hansen, T. Plewa, N. Hearn, D. Arnett, and J.C. Wheeler. Modeling of multi-interface, diverging, hydrodynamic experiments for the national ignition facility. *Astrophysics and Space Science*, 322(1–4):57–63, 2009.

[3] RJ ADRIAN. PARTICLE-IMAGING TECHNIQUES FOR EXPERIMENTAL FLUID-MECHANICS. *ANNUAL REVIEW OF FLUID MECHANICS*, 23:261–304, 1991.

[4] N.E. Lanier, C.W. Barnes, R. Perea, and W. Steckle. Feasibility of fluorescence-based imaging of high-energy-density hydrodynamics experiments. *Review of Scientific Instruments*, 74(3):2169–2173, 2003.

[5] B.L. Haendler, S.R. Buckley, C. Chen, A.R. Cook, R.C. Cook, L.M. Hair, F.M. Kong, H.D. Kramer, S.A. Letts, G.E. Overturf III, D.L. Schumann, and R.S. Upadhye. Low-density hydrocarbon foams for laser fusion targets. Technical report, LLNL, 1988.

[6] M.J. Berger, J.H. Hubbell, S.M. Seltzer, J. Chang, J.S. Coursey, R. Sukumar, D.S. Zucker, and K. Olsen. XCOM: Photon cross sections database, 2012.

[7] E.J. Gamboa. X-ray fluorescence experiments on trident. 2011.

[8] S.B. Hansen, A.Ya. Faenov, T.A. Pikuz, K.B. Fournier, R. Shepherd, H. Chen, K Widmann, S.C. Wilks, Y. Ping, H.K. Chung, A. Niles, J.R. Hunter, G. Dyer, and T. Ditmire. Temperature determination using Kα spectra from M-shell Ti ions. *Physical Review E*, 72(036408), 2005.